Journal of the European Ceramic Society 20 (2000) 357–366

Phase relationships and microstructures of Ca and Al-rich α-sialon ceramics

C.A. Wood, Y.-B. Cheng*

Department of Materials Engineering, Monash University, Melbourne, VIC 3168, Australia

Received 18 January 1999; received in revised form 26 May 1999; accepted 5 June 1999

Abstract

Ca sialon compositions rich in Al and Ca were fabricated and characterised in this work. Sintered compositions are found to be dominated by AlN′ and AlN-polytypoid phases. Large quantities of grain boundary glass are also present. Analysis of crystalline phases provided phase assemblage information for compositions with high *m* and *n* values and led to the refinement of an existing phase behaviour diagram. A modified phase behaviour diagram incorporating the current work has been proposed. Microstructural and fracture surface features are examined by a scanning electron microscope (SEM). a Sialon grains in these compositions have been observed with an elongated morphology. © 2000 Elsevier Science Ltd. All rights reserved.

Keywords: AlN; Grain boundaries; Microstructure-final; Phase equilibria; Sialon

1. Introduction

Until recently, the development of single phase α-sialon (α′) ceramics has received little attention. This has primarily been due to their poor fracture toughness and processing difficulties associated with their fabrication. Contrasting this, β-sialon (β′) ceramics have been extensively developed. β-Sialons are easily densified by pressureless sintering and display a combination of desirable properties. Significant among these is the relatively high fracture toughness of β-sialon, which arises from the in situ growth of β-sialon grains with an elongated morphology. It is well established that the presence of high aspect ratio elongated grains gives rise to mechanisms such as crack deflection, crack bridging and grain pullout which improve fracture toughness and reliability.[1]

α-Sialon compositions lie on a plane described by the equation $Me_xSi_{12-(m+n)}Al_{m+n}O_nN_{16-n}$ [Eq. (1)] for a metal ion Me^{v+}, where $x=m/v$ and is $\leqslant 2$. The cation Me may be Li, Mg, Ca, Y and some rare earth metals. α-Sialon has generally been considered to occur with an equiaxed grain morphology.[2,3] This gives α-sialon inferior fracture toughness relative to β-sialon. α-Sialon has a considerably higher hardness than β-sialon, making it a better material for high wear applications.[4] However, because of its poor fracture toughness, high temperature phase instability and processing difficulties, α-sialon generally finds use only as a minor phase in α-/β-sialon composites, where the hardness of the α′ phase supplements the toughness of the β′ phase.

Recent work by a number of researchers has described the anisotropic growth of α-sialon grains during sintering.[5–7] In almost all cases, the fabrication of ceramics featuring elongated α-sialon grains has required pressure sintering techniques. This has obvious cost and processing disadvantages in a commercial situation. Previous work by us has shown that in the Ca α-sialon system, elongated α-sialon grows readily during pressureless sintering.[8,9] Significant interest lies in developing elongated α-sialon microstructures as they hold promise for fabricating materials with very high hardness combined with improved fracture toughness that may result from the in situ growth of elongated grains.

To date, little study has been done on the Ca α-sialon system when compared to the yttrium and rare earth systems. A region of the Ca α-sialon phase behaviour diagram has been investigated in detail by Hewett et al., though in this work compositions were limited to a range of low *m* and *n* values in the Ca α-sialon equation [Eq. (1)].[10] Anisotropic grain growth is found to occur

* Corresponding author.

PII: S0955-2219(99)00164-8

in higher m and n value Ca α-sialon compositions,[8,11] however, only a small number of these compositions have been studied. Large regions of the phase behaviour diagram remain unexplored and, therefore, it is desirable to characterise these regions in order to gain a more complete understanding of this significant system. Additionally, earlier work has shown a tendency for α-sialon grain lengths and aspect ratios to increase with increasing m-value.[12] The microstructural characterisation of a wide range of compositions would provide opportunity for examining whether any of the microstructures were particularly suited to in situ toughening.

The work presented here examined eight high m and n value Ca α-sialon compositions. Compositions were selected to cover a broad region of the Ca α-sialon phase behaviour diagram. Results relating to phase assemblages and microstructures of the various compositions are discussed. Features related to fracture surfaces of the materials were also examined.

2. Experimental procedures

Eight samples covering a broad range of compositions were examined in this work. The compositions, listed in Table 1, were designed to nominally lie on the two-dimensional α-sialon plane described by Eq. (1). Locations of the compositions on the plane are shown in Fig. 1. All eight compositions were Al- and Ca-rich and were situated outside the single phase α-sialon region on the α-sialon plane (Fig. 2).

Samples are designated by their m and n values in Eq. (1) according to their positions on the α-sialon plane, where the name CA2040 refers to a design composition with $m=2$ and $n=4$, and so on. Compositional corrections were made to account for the presence of surface oxides on the starting powders.

Powders of Si_3N_4 (Starck, LC10, 1.94 wt% oxygen), AlN (Starck, Grade B, 2 wt% oxygen), $A1_2O_3$ (Ajax Chemicals, Sydney) and $CaCO_3$ (Ajax Chemicals, Sydney) were hand mixed with isopropanol using a mortar and pestle. Subsequent to mixing the slurry was dried and hand mixed again. Approximately 4 g of powder was then uniaxially pressed into 14 mm diameter pellets, followed by cold isostatic pressing at 200 MPa. Prior to sintering, specimens were calcined in a graphite furnace at 900°C for 1 h under vacuum to decompose $CaCO_3$ to CaO. For sintering, pellets were packed in a 50 wt% Si_3N_4: 50 wt% BN powder bed inside a graphite crucible. The pellets were then pressureless sintered in a graphite resistance furnace in a nitrogen atmosphere for 2 h at 1800°C. Furnace heating rates were 30°C/min to 1000°C and 10°C/min thereafter. Cooling took place in the furnace by switching off power after sintering which gave a cooling rate of ~40°C/min from 1800 to 1500°C and ~25°C/min below 1500°C.

Table 1
Design m and n-values and powder compositions (wt%) of the eight samples studied in this work

Sample	m-Value	n-Value	Si_3N_4	AlN	CaO	Al_2O_3
CA2040	2.0	4.0	46.94	30.04	9.31	13.70
CA2050	2.0	5.0	39.06	32.09	9.30	19.56
CA3040	3.0	4.0	37.93	38.05	13.54	10.49
CA3050	3.0	5.0	30.30	40.02	13.52	16.16
CA4040	4.0	4.0	29.44	45.58	17.51	7.46
CA4050	4.0	5.0	22.05	47.49	17.49	12.97
CA5040	5.0	4.0	21.45	52.68	21.26	4.61
CA5050	5.0	5.0	14.28	54.52	21.23	9.96

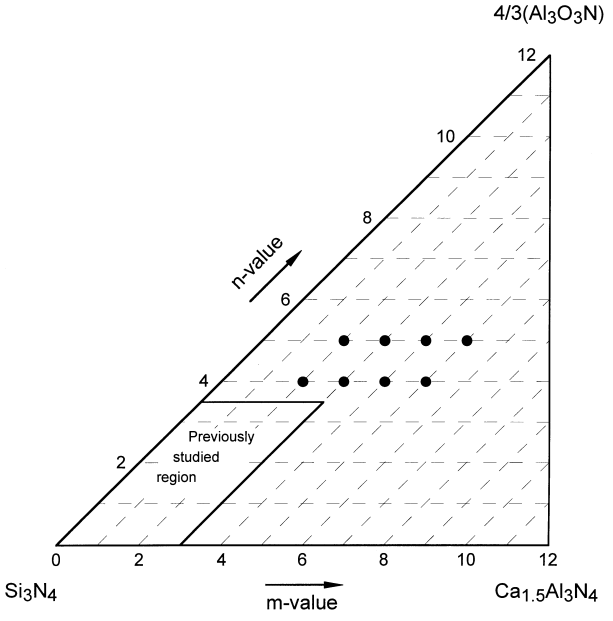

Fig. 1. Positions of the eight designed compositions on the Ca α-sialon plane defined by the formula $Ca_{m/2}Si_{12-(m+n)}Al_{m+n}O_nN_{16-n}$, also showing the region previously studied by Hewett et al.[10]

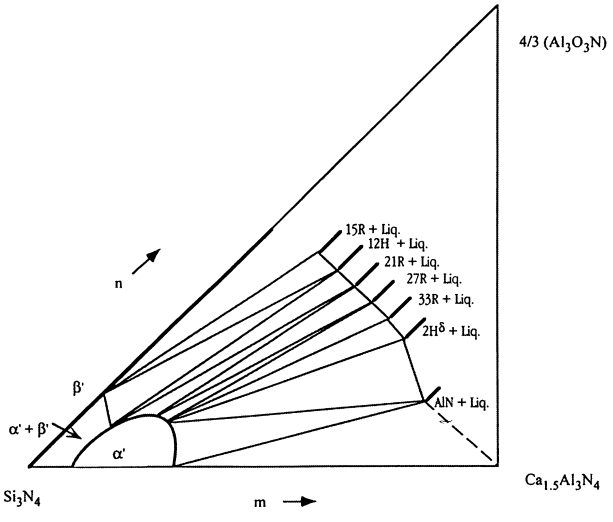

Fig. 2. Ca α-sialon phase behaviour diagram published by Hewett et al.[10]

Weight loss of samples was recorded after sintering. Bulk densities were determined by Archimedes' principle after the samples were boiled in water for 1 h and cooled to room temperature. Phase identification was performed on a Rigaku-Geigerflex X-ray diffractometer (XRD) using Ni-filtered CuK_α radiation. Lattice parameter measurements were obtained using XRD and the CELSIZ program.[13] A Si standard was used to calibrate peak positions before being processed by CELSIZ. Microstructural observations of both etched and fracture surfaces were performed on a JEOL JSM-840A scanning electron microscope (SEM). Polished sample surfaces were etched by immersion in molten NaOH for 10 s to remove grain boundary glass and then carbon coated prior to SEM observation. Fracture surfaces were gold coated. Energy dispersive X-ray spectroscopy (EDXS) was utilised on the SEM to chemically analyse specific microstructural features in the etched samples.

3. Results and discussion

Weight loss and bulk density data are presented in Table 2. Accurate measurements of samples CA4050, 5040 and 5050 could not be carried out due to extensive bloating of the pellets during sintering. The bloating resulted from the rapid evolution of large quantities of liquid phase that occurred during the heating of the pellets.

3.1. Crystalline phase development

The eight compositions studied in the present work were all Al and Ca rich. Examination of the phase behaviour diagram proposed by Hewett et al.[10] (Fig. 2) suggested that the sintered samples would contain increasing proportions of AlN and/or AlN-polytypoid phases and relatively small quantities of α-sialon as these compositions were located further from the single phase α-sialon region. XRD results confirmed that this was indeed the case. Table 3 displays the crystalline phases present in the eight samples.

Table 2
Weight loss and density of Ca α-sialon samples after sintering for 2 h at 1800°C

Sample	Weight loss (%)	Density (gcm^{-3})[a]
CA2040	0.68	2.690
CA2050	1.19	2.570
CA3040	0.72	2.673
CA3050	1.22	2.529
CA4040	3.01	2.838
CA4050	–	–
CA5040	–	–
CA5050	–	–

[a] All errors in density are ± 0.001 gcm^{-3}.

For reasons explained further on in this section, the AlN product phase was designated AlN′ in this work. All compositions except one contained α-sialon coexisting with AlN′ and/or AlN-polytypoid phases. The exception was the most Al-rich composition, CA5050, which exhibited AlN′ as the only crystalline phase. AlN-polytypoid phases are AlN defect structures that arise from the incorporation of silicon and oxygen into the AlN 2H structure. AlN′ and the polytypoid phases coexist with substantial quantities of liquid phase at the sintering temperature as the AlN-based phase regions on the α-sialon plane are the intersections of AlN (polytypoid)–liquid tie lines with the plane. The liquid forms an amorphous grain boundary phase upon cooling and is not readily detected by XRD. Identification of the polytypoid phases by XRD was difficult in some cases due to extensive peak overlapping with α-sialon and AlN′ in the spectrum.

Phase analysis revealed that α-sialon was not more than approximately 50% of crystalline phases (by XRD intensity) in the lower *m*-value compositions and was considerably less in the compositions located most distant from the single phase α-sialon region. Decreases in α-sialon were accompanied by increases in the observed quantities of AlN′ and/or AlN-polytypoid phases. XRD results showed that the type of AlN-polytypoid phases present in the samples varied significantly with composition. Within the eight compositions under investigation, five AlN-based phases were identified. This resulted from the close proximity of the AlN-polytypoid phases to one another on the phase behaviour diagram, whereby small changes in the *m* and *n* values caused substantial variations in the type and quantity of polytypoid phases observed.

The manner in which the polytypoid phases varied was consistent with the phase compatibility triangles on the behaviour diagram constructed by Hewett et al.[10] However, the actual phases that evolved from a given composition differed from the ones predicted by the

Table 3
Crystalline phases of Ca α-sialon samples after sintering for 2 h at 1800°C[d]

Sample	α′[a]	AlN′[b]	12H[c]	21R[c]	27R[c]	2H$^{\delta}$[c]
CA2040	vs	–	tr	s	–	–
CA2050	ms	–	vs	mw	–	–
CA3040	m	–	–	mw	vs	–
CA3050	mw	–	–	mw	vs	–
CA4040	m	vs	–	–	–	s
CA4050	w	vs	–	–	–	m
CA5040	w	vs	–	–	–	–
CA5050	–	vs	–	–	–	–

[a] α′ = α-sialon.
[b] AlN′ = aluminium nitride solid solution.
[c] 12H, 21R, 27R and 2H$^{\delta}$ = AlN-polytypoids.
[d] X-ray peak intensities: s = strong, m = medium, w = weak, v = very strong, tr = trace.

diagram. The diagram in Fig. 2 was constructed from Ca α-sialon compositions with *m* and *n* values no greater than 3 and 3.5, respectively. No compositions with higher *m* and *n* values were studied. Consequently, while the diagram is correct for lower *m* and *n* value compositions, it becomes less accurate when it is employed for higher *m* and *n* values. The present results provide supplementary phase information for the high *m* and *n* value compositions. Therefore, they can be used in conjunction with the results of Hewett et al. to produce a more precise phase behaviour diagram (Fig. 3), drawing from a broader range of compositions than previously done.

Included on this modified diagram is a region of AlN solid solution designated AlN′. This phase, which has been observed in some Ca α-sialon compositions,[8] closely resembles AlN on XRD spectra and TEM electron diffraction patterns.[9] Lattice parameter measurements (Table 4) also show the phase to have unit cell dimensions comparable to those for AlN. However, EDXS analysis of this phase (Fig. 4) revealed a small quantity of silicon to be present. This apparent substitution was consistently observed over a large number of grains, though a possibility exists that the silicon that was detected arose from other phases in the multiphase sample. In earlier work on a similar AlN phase this same apparent substitution was also observed using the better resolution of an EDXS equipped TEM on a thin foil sample.[9] It is hypothesised that this phase is an AlN solid solution in which small quantities of silicon and oxygen, less than that required to form the $2H^{\delta}$ polytypoid, are substituted into the AlN 2H structure. Consequently, phases in this work determined to be AlN or AlN-like are designated AlN′. Further work to clarify the characteristics of this phase is required and is currently in progress.

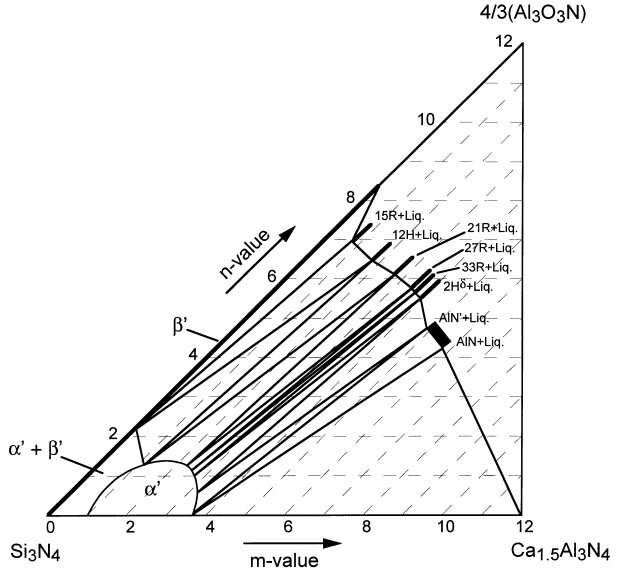

Fig. 3. Modified Ca α-sialon phase behaviour diagram constructed from phase information obtained by XRD in this work and work by Hewett et al.[10]

Table 4
Lattice parameters of AlN′ in sample CA5050 and pure AlN

Phase	Unit cell dimension (Å)	
	a	*c*
AlN′ in CA5050	3.112 ± 0.001	4.984 ± 0.003
Pure AlN[14]	3.111	4.979

3.2. Microstructural characterisation

Samples for SEM examination were polished and then chemically etched to remove residual grain boundary glass, allowing grain morphologies to be easily observed. For ease of reading, samples are discussed by their *m*-value groupings.

3.2.1. m = 2

Microstructural observations of samples CA2040 and 2050 [Figs. 5(a) and (b)] revealed microstructures displaying similar characteristics. XRD analysis of these samples established that they both had α-sialon coexisting with two AlN-polytypoid phases. However, SEM micrographs of the samples appear to show only two distinct crystalline phases. This resulted from the similar grain morphologies of the various polytypoids. The AlN-polytypoids all appear as long laths,[15] making exact identification difficult simply from SEM observation. Thus, though two polytypoids were present in a sample, microstructural observations appeared to reveal only one. The more important task of distinguishing between polytypoid phases and α-sialon was relatively easy as the chemical etching process utilised in this work generally gave the polytypoid phases a distinctive speckled appearance, while the α-sialon phase remained smooth. Additionally, when viewed edge-on, the polytypoid phases tended to be longer and have higher

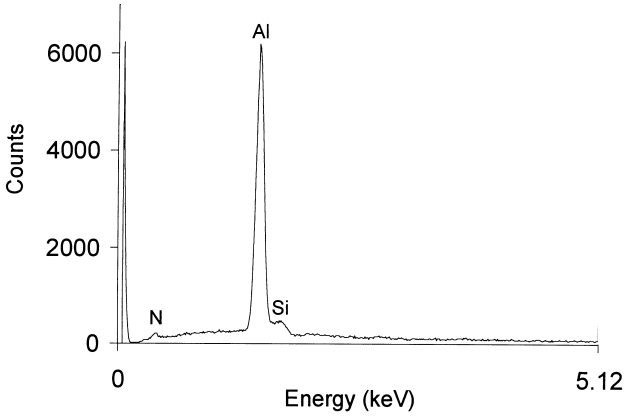

Fig. 4. EDXS spectrum of AlN′ phase in sample CA5050.

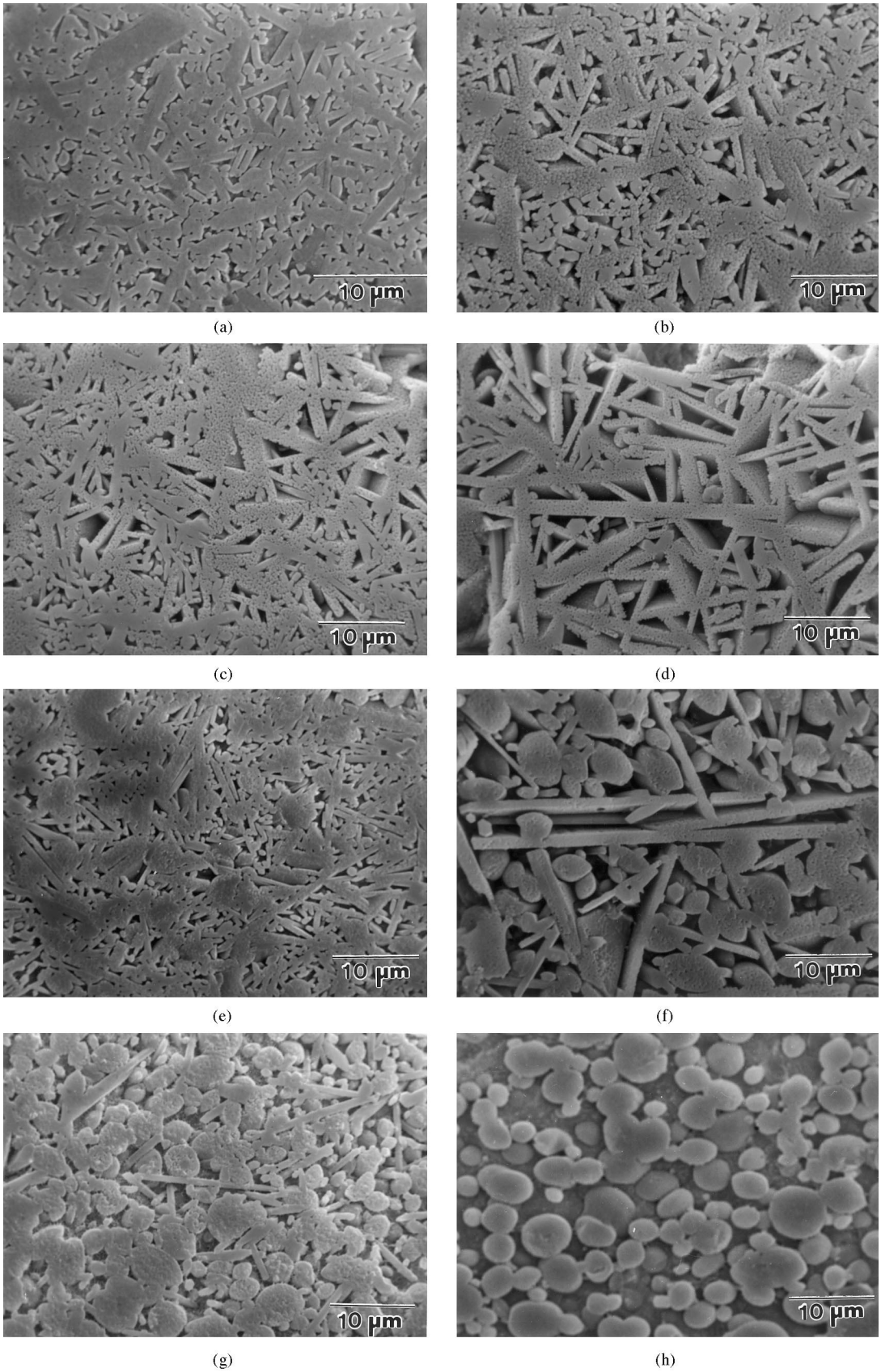

Fig. 5. Secondary electron micrographs of samples (a) CA2040, (b) CA2050, (c) CA3040, (d) CA3050, (e) CA4040, (f) CA4050, (g) CA5040 and (h) CA5050. The samples were etched in molten NaOH for 10 s before SEM observation.

aspect ratios than elongated α-sialon. EDXS spectra in Fig. 6 also shows the compositional diffierences between Ca α-sialon [Fig. 6(a)] and an AlN-polytypoid phase, in this case the 12H phase in CA2050 [Fig. 6(b)].

The majority polytypoid phase in CA2040 was 21R, while in CA2050 it was 12H. Cross-sections of the polytypoid laths averaged ~10 μm in length, though grains exceeding 20 μm were observed in the more liquid rich (*n*–5) compositions. The lath morphology of the polytypoid grains was unclear in some of the samples, with many grains appearing to display a more needle-like morphology. However, examination of pores in the samples clearly showed the lath morphology of the polytypoid phases (Fig. 7). The needle-like appearance of the polytypoid grains in many of the micrographs was due to the thin cross-section of the laths at most grain orientations. Only occasional grains that had an orientation approximately parallel to the sample surface clearly displayed the lath morphology. α-Sialon with an elongated morphology was present in both samples. The average grain length of α-sialon was about 5 μm in

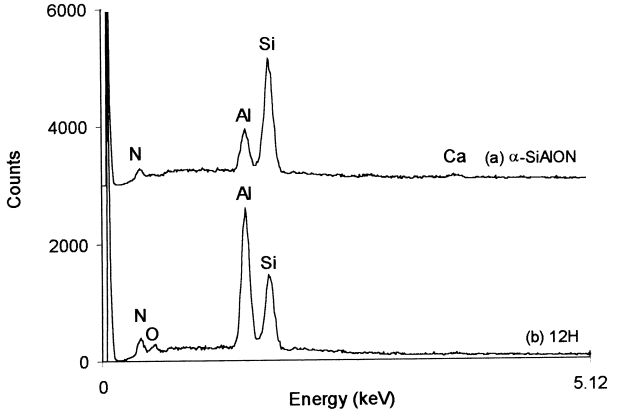

Fig. 6. EDXS spectra of (a) Ca α-sialon and (b) 12H polytypoid phases in sample CA2050.

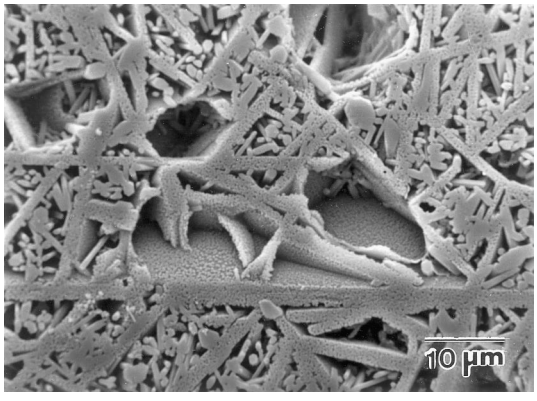

Fig. 7. Secondary electron micrograph of a pore in sample CA3040 showing the lath morphology of the polytypoid phase.

CA2040, with aspect ratios ranging from 3 to 8. Sample CA2050 contained significantly less α-sialon and the average length of α-sialon grains was smaller at about 3 μm. The smaller α-sialon grain size was attributed to the abundance of polytypoid in the microstructure. The large quantity of polytypoid plates formed a network, limiting the amount of space for elongated α-sialon to grow in. This caused α-sialon grain growth to be hindered as the anisotropically growing grains impinged on the large polytypoid plates. It is believed that this occurred by the growth of the polytypoid laths taking place prior to any extensive α-sialon grain growth.

3.2.2. m = *3*

Microstructures of samples CA3040 and 3050 bore some similarities to the $m=2$ samples discussed previously. Both compositions contained α-sialon and had 27R as the dominant polytypoid phase. Elongated α-sialon was featured in both samples. Sample CA3040 [Fig. 5(c)] appeared very much like CA2050, the most prominent difference being slightly larger elongated α-sialon grains. α-Sialon grains averaged ~5 μm in length, though a number of grains approaching 10 μm were observed. Sample CA3050 [Fig. 5(d)] was dominated by large, flat laths of polytypoid phases and a large volume of grain boundary glass. The laths averaged 10–15 μm in length with many exceeding 30 μm. Some elongated α-sialon was present, however it constituted only a minor component of the microstructure.

3.2.3. m = *4*

The m = 4 compositions [Figs. 5(e) and (f)], especially CA4050, were located a great distance from the single phase α-sialon region of the phase behaviour diagram and consequently, these compositions produced microstructures comprising primarily of AlN′/polytypoid and grain boundary glass phases. Both CA4040 and 4050 exhibited an AlN-type phase that had an equiaxed or globular morphology, contrasting the plate morphology observed in the samples discussed previously. This phase was the AlN′ identified by XRD. It should be noted that this globular phase was not the original AlN raw material, but rather was a new product phase. Both compositions also exhibited an elongated polytypoid phase coexisting with the globular AlN′. Exact identification of this phase by XRD was difficult due to peak overlaps on the XRD spectrum, however, based on the phase relationship outlined in Fig. 2 it was likely that this was the $2H^{\delta}$ phase. Significant quantities of small elongated α-sialon grains were observed in the CA4040 microstructure. The average grain length was in the range 2–3 μm, however, the small grains retained their high aspect ratio morphology. Sample CA4050 had a much higher glass content than CA4040. Crystalline phases were composed mostly of AlN′ and $2H^{\delta}$. The high glass content allowed the AlN′ and $2H^{\delta}$ to grow to

substantial dimensions, the most prominent feature being $2H^{\delta}$ laths exceeding 40 μm in length. Weak α-sialon peaks appeared on the CA4050 XRD spectrum and SEM confirmed its presence, however, the elongated α-sialon grains appeared only intermittently within the microstructure.

3.2.4. $m=5$

Sample CA5040 [Fig. 5(g)] was a liquid rich composition that evolved two very distinct crystalline phases, AlN′ and α-sialon. Within the abundant glass matrix, AlN′ grains with a distinctive elliptical morphology were seen as the majority phase. They exhibited diameters of 3–5 μm. The second crystalline phase observed in the microstructure was α-sialon. The large liquid volume at the sintering temperature combined with a lack of bulky polytypoid laths allowed α-sialon grains to grow relatively unhindered. This resulted in some α-sialon grains approaching 20 μm in length with aspect ratios of approximately 14. The average α-sialon grain length was about 8–10 μm. Composition CA5050 [Fig. 5(h)] was positioned outside any α-sialon containing compatibility triangle and exhibited AlN′ as the only crystalline phase. SEM micrographs show the sample to contain very large volumes of glass, so much so that adjacent AlN′ grains were barely in contact with one another. The AlN morphology was the same as described for sample CA5040, though the large liquid volumes allowed the grains to grow up to 8 μm in diameter. Chemical analysis of a grain in CA5050 by EDXS (Fig. 4) and lattice parameter measurements (Table 4) confirmed that the phase was the hypothesised AlN′ solid solution and not a polytypoid.

It is seen from the above results that one of the most significant microstructural features of the samples in this work was the elongated morphology of the α-sialon phase over a wide range of compositions. Earlier work by us[11] has suggested that in Ca α-sialon compositions with a design *m*-value more than ~2, α-sialon has an intrinsically elongated grain morphology. The development of α-sialon grains with an elongated shape is further facilitated by the increasing amount of glassy phase that occurs in samples with higher *m*-values. All seven of the α-sialon containing compositions in this work exhibited elongated α-sialon, adding further evidence to the belief that anisotropic α-sialon grain growth is an intrinsic feature of the calcium sialon system. No equiaxed α-sialon was observed in any of the microstructures.

Interest in in situ toughened α-sialon ceramics is increasing as the materials can possess fracture toughness comparable to β-sialon while retaining the very high hardness of the α-sialon phase. While providing valuable phase information, the compositions studied in this work would feature very poor hardness because of the low α-sialon and high glass contents they possessed.

3.3. Fracture surfaces

Fracture surfaces of the samples under investigation were obtained in order to observe the effects that different phases would have on the fracture behaviour. Earlier work by us showed that compositions dominated by elongated α-sialon displayed R-curve behaviour and improved fracture toughness.[8] Fracture surfaces of these materials showed evidence of microstructural toughening mechanisms such as grain debonding and grain pullout (Fig. 8). The purpose of SEM observation of the current samples was to determine how large volumes of glass phase and AlN′/polytypoid phases altered the fracture surface characteristics.

Of the eight samples, compositions CA2040 and 3040 contained the least grain boundary glass. Examination of their respective fracture surfaces [Fig. 9(a) and (c)] showed some evidence of grain debonding and pullout. Like their polished and etched microstructures, their fracture surfaces bore some similarities. These two compositions contained prominent elongated α-sialon grains and this was reflected in their fracture surfaces. Features such as needle shaped imprints and elongated grains standing proud of the surface indicated potential toughening mechanisms attributable to α-sialon grains. Contrasting this, sample CA2050 [Fig. 9(b)] had a very angular fracture surface. This was attributed to the large polytypoid content and small α-sialon grain size of this sample. Fracture around the laths produced a jagged surface combined with smooth regions where large laths had debonded from the glass matrix. Laths of polytypoid were seen projecting out of the fracture surface, raising the possibility that the debonding of this phase may also contribute to in situ toughening.

The strength of the grain–glass interface is important in determining the effectiveness of abnormally grown grains in promoting in situ toughening. In situ toughening relies on an interfacial bond that is weak enough

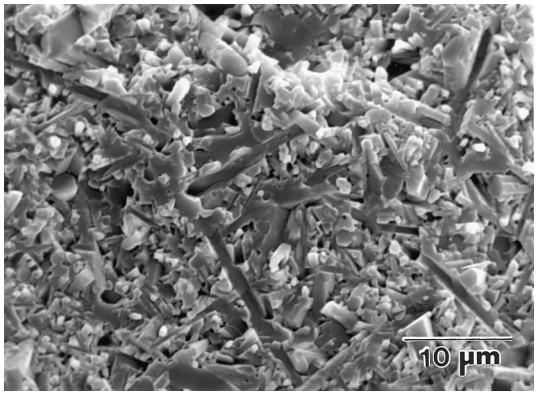

Fig. 8. Secondary electron micrograph of fracture surface from Ca α-sialon with $m=3$, $n=1.5$.[8]

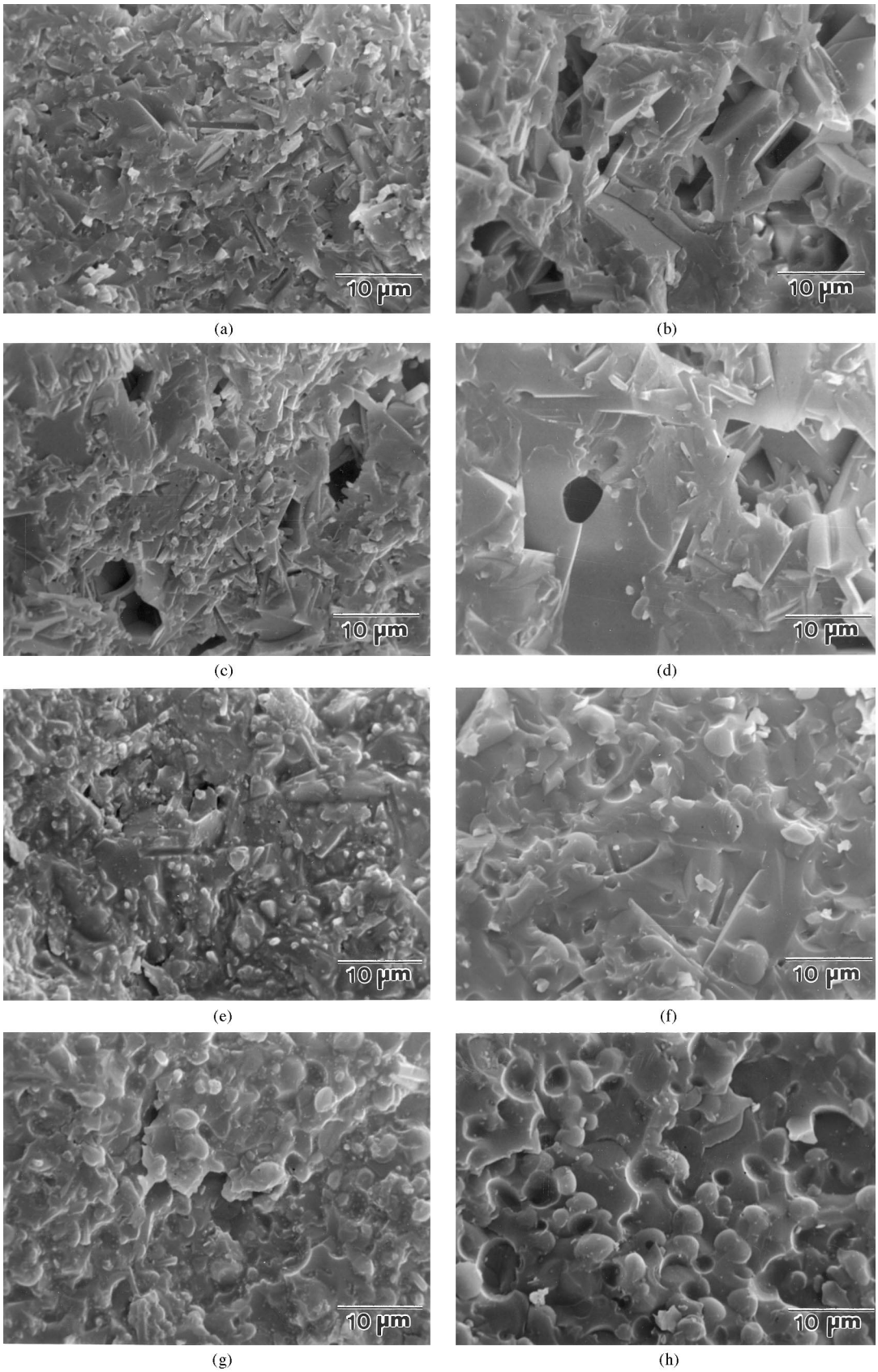

Fig. 9. Secondary electron micrograph of fracture surfaces of samples (a) CA2040, (b) CA2050, (c) CA3040, (d) CA3050, (e) CA4040, (f) CA4050, (g) CA5040 and (h) CA5050.

to debond and deflect a propagating crack, resulting in intergranular fracture. If the bond is too strong, a crack fractures the grain rather than being deflected around it (i.e. transgranular fracture) and the grain makes no contribution to improving fracture toughness. The effect of a strong interfacial bond was apparent in sample CA3050 [Fig. 9(d)]. Evidence of cracks propagating through the plates rather than debonding them from the matrix was observed, indicating a strong bond between the extensive network of polytypoid plates and the relatively large quantity of glass matrix. Only plates with an orientation roughly parallel to the fracture surface readily debonded. This observation was consistent with our earlier work which showed that microstructures containing large quantities of high aspect ratio elongated α-sialon combined with a large volume of grain boundary glass did not exhibit improved fracture toughness.[8] This behaviour was attributed to a strong interfacial bond between Ca α-sialon and the calcium aluminosilicate glass.

Fracture surfaces of the $m=4$ and 5 samples showed little evidence of any type of toughening mechanisms, consistent with the very high glass contents observed in the microstructures. SEM micrographs of these samples revealed surfaces with a glassy appearance. A few debonded α-sialon grains were observed in the $m=4$ samples [Fig. 9(e) and (f)], however, when grain debonding did occur, it mostly involved globular shaped AlN′ grains which would provide little hindrance to crack propagation. This type of feature was particularly apparent in samples CA5040 and 5050 [Fig. 9(g) and (h)] which were dominated by globular AlN′ grains and glass phase.

Comparing the microstructures and fracture surfaces of these eight samples to compositions located closer to the single phase α-sialon region of the phase behaviour diagram,[8] it was evident that high *m*- and *n*-value compositions held little potential for the design of in situ toughened Ca α-sialon ceramics. This was directly related to the large volumes of glass in the microstructures. Firstly, the substitution of α-sialon for large volumes of glass phase would lead to significant deterioration in properties such as hardness and high temperature creep. Secondly, compositions dominated by grain boundary glass exhibited a strong tendency toward transgranular fracture, a mechanism that would not lead to improved fracture toughness. Compositions abundant in globular AlN′ grains exhibited intergranular fracture, however, this grain morphology does not appreciably alter the crack path or require significant energy to debond the grain–glass interface. Therefore, based on this and earlier work, it is reasonable to conclude that considerable improvements in the fracture toughness of ceramics in the Ca α-sialon system require microstructures containing anisotropically grown grains combined with a relatively small volume of grain boundary glass.

4. Conclusion

The phase and microstructural development of eight high *m* and *n* value Ca α-sialon compositions were examined in this work. Compositions were located in previously unstudied regions of the phase behaviour diagram. Phase analysis indicated decreases in the quantity of α-sialon and increases in AlN′ and/or AlN-polytypoid phases with increasing composition *m* and *n* values. Grain boundary glass also increased with increasing *m* and *n* values and was a major constituent of the microstructures in the $m=4$ and 5 compositions. Utilising the additional phase information provided by this work to supplement earlier work on the system, a modified phase behaviour diagram was proposed. α-Sialon was observed with an elongated morphology in the seven compositions that contained the phase. AlN-polytypoid phases were seen to be present as large laths. Large quantities of these phases were seen to interfere with the growth of α-sialon through steric hindrance. An examination of fracture surfaces saw some evidence of toughening mechanisms in lower *m* and *n* value compositions, however compositions dominated by grain boundary glass and globular AlN′ presented no features to suggest possible mechanisms of in situ toughening.

References

1. Hoffmann, M. J., Analysis of microstructural properties of Si_3N_4 ceramics. In *Tailoring of Mechanical Properties of Si_3N_4 Ceramics*, ed. M. J. Hoffmann and G. Petzow. Kluwer Academic Publishers, 1994, pp. 59–72.
2. Cao, G. Z. and Metselaar, R., α′-SiAlON ceramics: a review. *Chem. Mater.*, 1991, **3**(2), 242–252.
3. Ekström, T. and Nygren, M., SiAlON Ceramics. *J. Am. Ceram. Soc.*, 1992, **75**(2), 259–276.
4. Ekström, T., α-SiAlON and α-/β-SiAlON composites: recent research. In *Engineering Ceramics '96. Higher Reliability through Processing*, ed. G. N. Babini, M. Haviar and P. Sajgalik. Kluwer Academic Publications, 1997, pp. 147–167.
5. Wang, H., Cheng, Y.-B., Muddle, B. C., Gao, L. and Yen, T. S., Preferred orientation in hot-pressed Ca α-SiAlON ceramics. *J Mater. Sci. Lett.*, 1996, **15**(16), 1447–1449.
6. Shen, Z. J., Nordberg, L.-O., Nygren, M. and Ekström, T., α-SiAlON grains with high aspect ratio — utopia or reality? In *Engineering Ceramics '96. Higher Reliability through Processing*, ed. G. N. Babini, M. Haviar and P. Sajgalik. Kluwer Academic Publications, 1997, pp. 169–178.
7. Chen, I.-W. and Rosenflanz, A., A tough SiAlON ceramic based on α-Si_3N_4 with a whisker-like structure. *Nature*, 1997, **389**, 701–704.
8. Wood, C. A., Zhao, H. and Cheng, Y.-B., Microstructural development of Ca α-SiAlON ceramics with elongated grains. *J. Am. Ceram. Soc.*, 1999, **82**(2), 421–428.
9. Zhao, H., Swenser, S. P. and Cheng, Y.-B., Elongated α-Sialon grains in pressureless sintered sialon ceramics. *J. Eur. Ceram. Soc.*, 1998, **18**(8), 1053–1057.
10. Hewett, C. L., Cheng, Y.-B., Muddle, B. C. and Trigg, M. B., Phase relationships and related microstructural observations in the Ca–Si–Al–O–N system. *J. Am. Ceram. Soc.*, 1998, **81**(8), 1781–1788.
11. Wood, C. A., Zhao, H. and Cheng, Y.-B., Effects of composition on the morphology of α-sialon ceramics. To be published in *The*

Proceedings of the Ist China International Conference on High-Performance Ceramics, Beijing, China, 1998.
12. Wood, C. A., Zhao, H. and Cheng, Y.-B., In situ toughening of α-SiAlON ceramics. In *The Proceedings of Materials '98*, ed. M. Ferry. The Inst. of Mater. Eng., Wollongong. 1998, Vol. 2, pp. 663–668.
13. Scott, H. G., CELSIZ program, *CSIRO*, 1986.
14. JCPDS powder diffraction file #25-1133, JCPDS-International Centre for Diffraction Data, 1995.
15. Jack, K. H., Review: sialons and related nitrogen ceramics. *J. Mat. Sci.*, 1976, **11**, 1135–1158.